

# Supplementary Information

## Derivation of the Dynamic Saturation Model

The principle of electrowetting-on-dielectric (EWOD) operation is described by the Lippmann equation [1]:

$$\cos\theta(V) = \cos\theta(0) + \frac{1}{2} \frac{\varepsilon_0 \varepsilon}{d\gamma} V^2 \quad (\text{S1})$$

where  $d$  is the thickness of the dielectric layer and  $\gamma$  is the surface tension between liquid and gas interface.  $\varepsilon_r$  and  $\varepsilon$  are the relative permittivity of the dielectric and the vacuum permittivity, respectively.  $\theta(0)$  and  $\theta(V)$  are the contacting angle before and after voltage is applied.

When the droplet is transported on the open digital microfluidics (DMF) chip, Equation (S1) should be changed to [2]:

$$\cos\theta(V) = \cos\theta(0) + \frac{1}{2} \frac{\varepsilon_0 \varepsilon}{d\gamma} \left(\frac{V}{2}\right)^2 \quad (\text{S2})$$

because the voltage of source is evenly applied on the two identical capacitors (shown in Figure S1).

In EWOD applications, the radius of droplet should not be larger than 1 mm, below which the surface tension dominates the droplet and the influence of gravity can be neglected. According to three-contact-line theory [3], the electrowetting force is calculated by the product of  $f_{dr}$  and effective contact line length  $l$  on the activated electrode. Besides, the hysteresis effect [4] in the EWOD surface should be taken into account, which is assumed to be a constant  $\Delta f$ . Therefore, the net electrowetting force is rewritten in the following expression [6].

$$F_{dr} = f_{dr}l - \Delta f = \frac{1}{8} \frac{\varepsilon_0 \varepsilon l}{d} V^2 - \Delta f \quad (\text{S3})$$

Herein, effective contact line length  $l$  is determined by the boundary structure formation of the adjacent electrodes. Specially, when the droplet moves, the contact line length varies with the droplet positions on the electrodes as shown in Figure S2c.

When the droplet moves from one electrode to the next adjacent one, its contact line length on the activated electrode varies from initial length  $x_0$  to  $l$ . Take a careful inspection of the process, the contact line length can be expressed as:

$$l(x) = 2\sqrt{2Rx - x^2} \quad (\text{S4})$$

For simplification, the average effect line length is calculated as the following.

$$l_{eff} = \int_{x_0}^l l(x) dx / l \quad (\text{S5})$$

Here,  $x$  represents the displacement of droplet on the device, and  $l = 2R$ .

For an optimized droplet motion effect,  $x_0$  is usually set in the range of  $[0.2l, 0.3l]$ . The responding values of effective contact line length are listed in the following Table S1.

**Table S1.** Effective contact line length varies with the initial contact line length.

|           |         |         |         |         |         |         |
|-----------|---------|---------|---------|---------|---------|---------|
| $x_0$     | $0.2l$  | $0.22l$ | $0.24l$ | $0.26l$ | $0.28l$ | $0.3l$  |
| $l_{eff}$ | $0.67l$ | $0.65l$ | $0.64l$ | $0.62l$ | $0.60l$ | $0.58l$ |

For simplification, the value of  $l$  is set as  $0.6l$ , i.e., sixty percent of the electrode width.

When the droplet moves, it suffers damping forces due to the friction in interfaces. The damping force from surrounding medium such as air or silicone oil is relatively weak and neglected. The primary damping force is caused by the surface of EWOD device. For parallel-plate configuration, the viscous drag force between the plates and the droplet is expressed as [5–7]:

$$F_{dm} = 2C_V \frac{\mu U}{h} S \tag{S6}$$

where  $C_V$  is an empirical constant in the range of 10~15 [9].  $h$  is the distance between the top and bottom plates of the parallel-plates EWOD, and  $S$  represents the droplet covering area on the EWOD device.

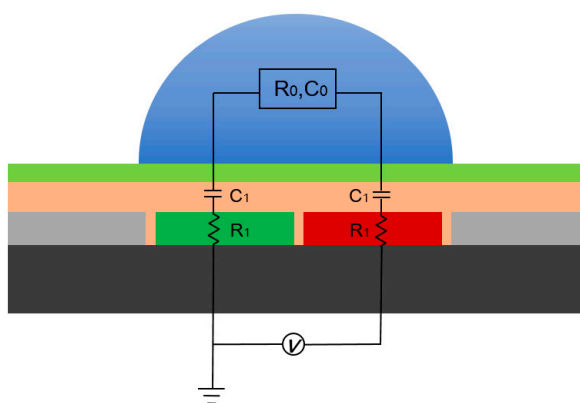


**Figure S1.** Equivalent electric circuit of the single-plate EWOD device. The dielectric layer is modeled as a capacitance  $C_1$ , the electrode is modeled as a resistance  $R_1$ , and the droplet is considered as a function of resistance  $R_0$  and capacitance  $C_0$ .

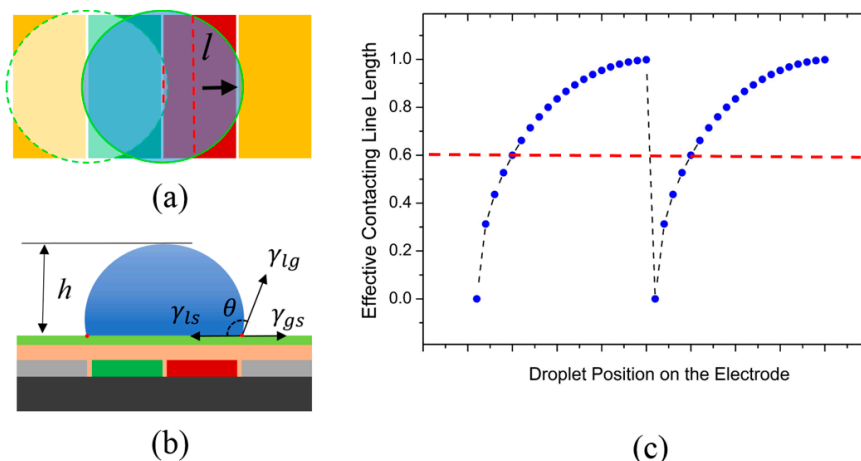


**Figure S2.** (a) The top view of the single-plate EWOD device. When the droplet moves from the initial position (left) to the equilibrium position (right), the contact line length (red line) is a function of droplet displacement on the electrode which changes in range of  $(0.2l, 0.3l)$ . (b) The side view of the single-plate EWOD device, wherein the red stands for the activated electrode, and the green stands for the grounded electrode. (c) The effective contact line length variation with the droplet position which changes in the advancing direction. The red dash line represents the average value of varied contact line length. Note that the value in (c) represents the normalized contact length to the electrode width.

For the droplet transported on a single-plate EWOD,  $h$  could be replaced with the droplet height (see the Figure S2b) since the device lacks the top plate. Thus the damping force on single-plate EWOD is written as:

$$F_{dm} = C_v \frac{\mu U}{\alpha R} S \quad (S7)$$

Here,  $R$  is the radius of the droplet, and  $\alpha R$  is the droplet height.  $\alpha$  is a parameter related to the contact angle. We assume that the droplet keeps spherical and experiences symmetrically deformation. The initial contact angle of the droplet on the hydrophobic surface is assumed to be 120 degree.

$$S = \pi R^2 \sin^2 \theta_c \quad (S8)$$

$$F_{dm} = K_c C_v \frac{\mu U}{\alpha R} S \quad (S9)$$

Meanwhile,  $R$  varies with the deformation of the droplet when driving voltage is applied. For simplicity, the influence of  $R$  variation in the modeling is neglected, which will be explained to be reasonable in the following.

In this study, we focus on the droplet motion on the single-plate EWOD device in ambient air. In this case, the damp force working on the droplet mainly comes from the bulk and from the moving contact line, which are of the same order of magnitude [7]. The contact angle hysteresis and damp effect in the triangle region are considered as manifestations of the pinning effect. Furthermore, pinning manifests itself as a stick-slip motion along the triple contact line for sessile droplets [8] and adversely affects the switching speed [9]. Thus, taking into account the pinning effect is necessary for making reasonable droplet dynamics model. Thus, the equation S6 should be rewritten as:

$$F_{dm} = K_c C_v \frac{\mu U}{\alpha R} S \quad (S10)$$

where  $K_c$  is the damp factor caused by the pinning effect in the triangle region, and is in the order of 2–4. Here, we assume it equals to three.

Combining Equations (S8) and (S9), Equation (S10) is written as the following:

$$F_{dm} = 2K_c C_v \mu U \pi R \cos^2 \left( \frac{\theta_c}{2} \right) \quad (S11)$$

To achieve droplet moving with a steady velocity on the open DMF chip there exists a dynamic equilibrium between driving force and damping force.

$$F_{dr} = F_{dm} \quad (S12)$$

Based on Equation (S12) a dynamic model of droplet transported on the single-plate EWOD is obtained, as shown below.

$$U = \frac{1}{16\pi R \mu K_c C_v} \frac{\epsilon_0 \epsilon_r V^2 l - 8\Delta f \cdot d}{d \cos^2 \left( \frac{\theta_c}{2} \right)} \quad (S13)$$

Combining Equations (S2) and (S13), the following equation is obtained:

$$U = \frac{\frac{\varepsilon_0 \varepsilon_r l}{d} \cdot V^2 - 8 \cdot \Delta f}{2\pi K_c C_v \mu R \left(2 + \frac{\varepsilon_0 \varepsilon_r l}{2d} \cdot V^2\right)} \quad (\text{S14})$$

The parameters values used in the calculations are presented in Table S2. When applied voltage is high enough, the influence of  $\Delta f$  can be neglected compared with the driving force, and Equation (S14) is simplified to be:

$$U = \frac{l}{2\pi K_c C_v \mu R d} \cdot \frac{1}{\frac{1}{2d} + \frac{2}{\varepsilon_0 \varepsilon_r V^2}} \quad (\text{S15})$$

To fit the experiment results, some difference between the theoretical and practical cases should be claimed. The velocity value reported in literature is obtained by dividing the length of an electrode by the transport time, which is the mean value. While the value induced by this model is the steady velocity, *i.e.*, the maximum. However, as shown in Figure S3a, the droplet transport experiences three basic process, including acceleration, steady migration, and deceleration. Thus, the mean transport velocity should be smaller than the steady one. The acceleration is related to the electrowetting process, which is not understood very clearly. But it's solid that this process costs a period of time, and the velocity increases until it reaches the steady state with maximum value. The deceleration of droplet also costs some time and finally comes to be still. Thus, it is reasonable to decrease the value predicted by this model by a factor,  $K_1$ , in the range of (1, 2). The value of  $K_1$  is determined by the time cost in acceleration and slow down process.

$$F_{dm} = K_1 K_c C_v \frac{\mu U}{\alpha R} S \quad (\text{S16})$$

$$U = \frac{\frac{\varepsilon_0 \varepsilon_r l}{d} \cdot V^2 - 8 \cdot \Delta f}{2\pi K_1 K_c C_v \mu R \left(2 + \frac{\varepsilon_0 \varepsilon_r l}{2d} \cdot V^2\right)} \quad (\text{S17})$$

Another error comes from the neglect of the radius change of droplet deformation. As Figure S3b shows, with the decrease of contact angle,  $R$  will become larger. But the variation of  $R$  is limited by the fact that the contact angle would get saturated in about  $80^\circ$  [10,11] and at this time the  $R$  keeps invariable.

**Table S2.** Parameter values used in Equation (S14).

| Parameters      | Value           |
|-----------------|-----------------|
| $d$             | 1 $\mu\text{m}$ |
| $\varepsilon_r$ | 7.8             |
| $\gamma$        | 72.6 mN/m       |
| $C_v$           | 12.5            |
| $\mu$           | 0.001 Pa·s      |
| $\Delta f$      | ~1.25 nN        |
| $l$             | 1 mm            |

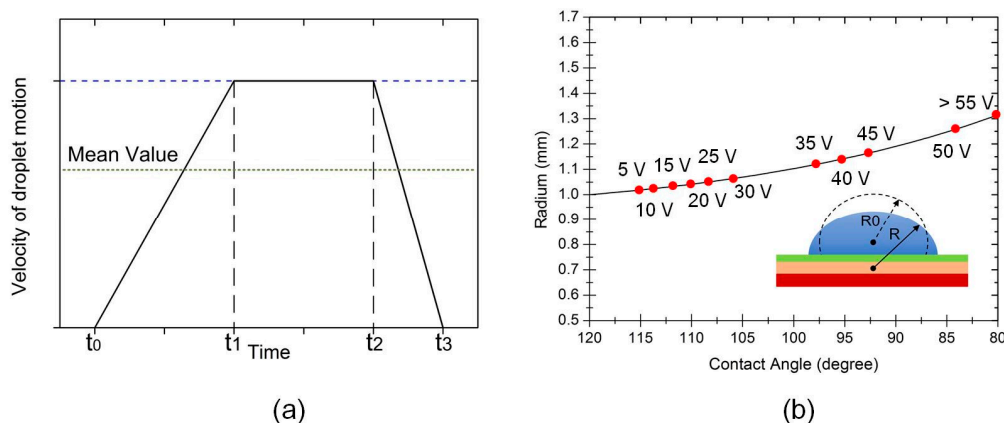


**Figure S3.** (a) The droplet velocity variation as a function of time; and (b) the droplet radius variation as the contact angle changes from 120 to 80 degree. Note that, the curve in (a) does not present the real case of the droplet motion process, but represents the acceleration, stable, and slow down processes in principle. The mean value is used as the measured value in reported literatures, and the stable one is utilized in this dynamic model. Besides, the red plots in (b) represent responding applied voltages of the contact angle, which gets saturated at the point of about 80 degree in voltages higher than 55 V due to the contact angle saturation effect [12].

## References

1. Vallent, M.; Berge, B.; Vovelle, L. Electrowetting of water and aqueous solutions on poly (ethylene terephthalate) insulating films. *Polymer* **1996**, *37*, 2465–2470.
2. Cui, W.; Zhang, M.; Zhang, D.; Pang, W.; Zhang, H. Island-ground single-plate electrowetting on dielectric device for digital microfluidic systems. *Appl. Phys. Lett.* **2014**, *105*, 013509.
3. Kang, K.H. How electrostatic fields change contact angle in electrowetting. *Langmuir* **2002**, *18*, 10318–10322.
4. Li, F.; Mugele, F. How to make sticky surfaces slippery: Contact angle hysteresis in electrowetting with alternating voltage. *Appl. Phys. Lett.* **2008**, *92*, 244108.
5. Brochard, F. Motions of droplets on solid surfaces induced by chemical or thermal gradients. *Langmuir* **1989**, *5*, 432–438.
6. Ren, H.; Fair, R.B.; Pollack, M.G.; Shaughnessy, E.J. Dynamics of electrowetting droplet transport. *Sens. Actuators B Chem.* **2002**, *87*, 201–206.
7. Song, J.H.; Evans, R.; Lin, Y.Y.; Hsu, B.N.; Fair, R.B. A scaling model for electrowetting-on-dielectric microfluidic actuators. *Microfluid. Nanofluid.* **2009**, *7*, 75–89.
8. Sen, P.; Kim, C.J. Capillary spreading dynamics of electrowetted sessile droplets in air. *Langmuir* **2009**, *25*, 4302–4305.
9. Yang, S.; Zhou, K.; Kreit, E.; Heikenfeld, J. High reflectivity electrofluidic pixels with zero-power grayscale operation. *Appl. Phys. Lett.* **2010**, *97*, 143501.
10. Yeo, L.Y.; Chang, H.C. Static and spontaneous electrowetting. *Mod. Phys. Lett. B* **2005**, *19*, 549–569.
11. Gupta, R.; Sheth, D.M.; Boone, T.K.; Sevilla, A.B.; Fréchet, J. Impact of pinning of the triple contact line on electrowetting performance. *Langmuir* **2011**, *27*, 14923–14929.

12. Mugele, F. Fundamental challenges in electrowetting: From equilibrium shapes to contact angle saturation and drop dynamics. *Soft Matter* **2009**, *5*, 3377–3384.

© 2015 by the authors; licensee MDPI, Basel, Switzerland. This article is an open access article distributed under the terms and conditions of the Creative Commons Attribution license (<http://creativecommons.org/licenses/by/4.0/>).